JOC The Journal of Organic Chemistry

Article

pubs.acs.org/joc

Deep-Red and Near-Infrared Xanthene Dyes for Rapid Live Cell Imaging

Guangle Niu,[†,‡] Weimin Liu,[*,†] Bingjiang Zhou,[†,§] Hongyan Xiao,[†] Hongyan Zhang,[†] Jiasheng Wu,[†] Jiechao Ge,[†] and Pengfei Wang[†]

[†]Key Laboratory of Photochemical Conversion and Optoelectronic Materials and CityU-CAS Joint Laboratory of Functional Materials and Devices, Technical Institute of Physics and Chemistry, Chinese Academy of Sciences, Beijing 100190, China

[‡]University of Chinese Academy of Sciences, Beijing 100049, China

Supporting Information

ABSTRACT: In this work, two xanthene dyes (**H-hNR** and **TF-hNR**) have been synthesized by a convenient and efficient method. These two dyes exhibited deep-red and near-infrared emissions, high fluorescence quantum yields, and good photostability. Their structure−optical properties were investigated by X-ray crystal structure analysis and density functional theory calculations. Live cell imaging data revealed that **H-hNR** and **TF-hNR** could rapidly stain both A549 and HeLa cells with low concentrations. The excellent photophysical and imaging properties render them as promising candidates for use in live cell imaging.

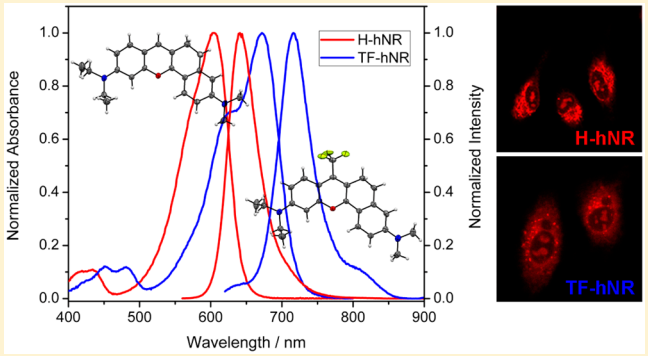

INTRODUCTION

In the past decades, fluorescence imaging based on small-molecule organic dyes has become a powerful tool to visualize biological events in living systems, such as biomolecule detection,[1] labeling,[2] and cancer diagnosis.[3] In contrast to fluorophores with emissions in short-wavelength regions, deep-red and near-infrared (NIR) fluorophores[4] are favored in in vivo bioanalysis and bioimaging due to decreasing light scattering and background autofluorescence, minimizing photodamage to biological samples, and improving tissue depth penetration.[5]

Xanthenes, mainly including fluoresceins and rhodamines, have been widely used in biological related applications owing to their outstanding photophysical properties.[6] However, classical xanthenes exhibit maximum emissions in visible regions, which results in low contrast in living systems. Substantial efforts have been made to synthesize xanthene derivatives with longer emission wavelengths. Early attempts to develop long-wavelength xanthene derivatives included introducing electron-withdrawing groups (CF_3, perfluorophenyl group, perfluoroalkyl group, and CN)[7] into the xanthene skeleton at position 9. Later, Lin and others developed several kinds of deep-red and NIR xanthene derivatives with moderate to high fluorescence quantum yields (QYs) by extending the π-conjugation of the xanthene skeleton.[8] Qian and Nagano et al.[9] innovatively proposed that replacing the bridged oxygen atom with other elements (Si, Ge, Sn, Te, or P) could convert traditional xanthenes to other derivatives with narrower energy gaps, resulting in much longer emission wavelengths and good fluorescence QYs.

Recently, the hybridization of two classical fluorescent dyes has also become a promising strategy for the design of long-wavelength fluorescent dyes.[10] For example, our group reported a family of coumarin-fused pyronin dyes (**CP** dyes) with deep-red emissions for subcellular organelle imaging.[11] However, the incubation concentrations of these **CP** dyes for imaging were in the range of 5−20 μM due to the low fluorescence QYs in Tris−HCl−EDTA (TE) buffer. The lactone group in the skeleton of **CP** dyes might be the main reason for their low fluorescence QYs, which was probably due to the strong interaction with polar solvent[12] and intramolecular charge transfer (ICT)[13] in coumarin parts. In addition, aggregation in polar solvent might also quench the fluorescence due to excellent planarity of **CP** dyes.[14] We suspected that replacement the lactone group in the skeleton of **CP** dyes with ethylene group could inhibit the above-mentioned factors, resulting in high fluorescence QY. In addition, introducing electron-withdrawing group (CF_3) could be utilized to develop NIR dye.[7b,15] Toward this end, we herein synthesized two xanthene dyes (**H-hNR** and **TF-hNR**) through effective condensation reaction and investigated their photophysical properties, X-ray crystal structure, density functional theory (DFT) calculations, and bioimaging properties in living cells.

Received: April 29, 2016
Published: August 3, 2016

DOI: 10.1021/acs.joc.6b00981
J. Org. Chem. 2016, 81, 7393−7399

Scheme 1. Synthesis of Deep-Red and NIR Dyes H-hNR and TF-hNR

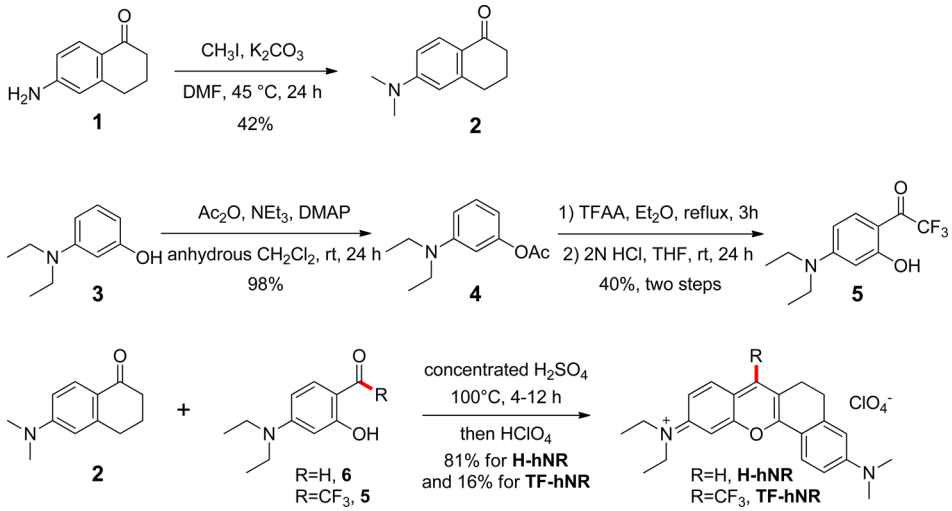

RESULTS AND DISCUSSION

Synthesis and Characterization. The synthesis routes of **H-hNR** and **TF-hNR** are outlined in Scheme 1. Compound **2** was synthesized through dimethylation of commercial available compound **1** with CH_3I and K_2CO_3 in DMF, and its synthesis was reported by our previous work.[16] Thus, **H-hNR** was synthesized by condensation reaction of compound **2** and commercial compound **6** in concentrated H_2SO_4 at 100 °C, with a high yield of 81%. Introducing electron-withdrawing group (CF_3) into the xanthene skeleton at position 9 can be utilized to develop new dyes with emissions in the NIR region.[7b,15] Compound **5** was obtained from commercial compound **3** via two steps. First, acetylation of compound **3** in anhydrous CH_2Cl_2 with Ac_2O produced compound **4**. A trifluoroacetyl group was introduced into compound **4** via the Friedel–Crafts reaction, and then deacetylation by 2 N HCl in THF led to the formation of compound **5**. Detailed information on the synthesis of compound **5** was reported in our another work.[15a] Similarly, compound **2** and compound **5** were heated at 100 °C in concentrated H_2SO_4 through a condensation reaction to produce **TF-hNR** (16%). The synthesized dyes (**H-hNR** and **TF-hNR**) were characterized by ^1H NMR, ^{13}C NMR, ^{19}F NMR, and HRMS.

Furthermore, the structures of **H-hNR** and **TF-hNR** were further confirmed by X-ray crystal structure analysis (Figures S1–S3, Supporting Information). The single crystals of **H-hNR** and **TF-hNR** were obtained by slow evaporation of the mixture solvent ($MeOH/CH_2Cl_2$ = 2:1, v/v) at ambient temperature. The details of the X-ray experimental conditions, cell data, and refinement data of **H-hNR** and **TF-hNR** are summarized in Tables S1 and S2 of the Supporting Information. **H-hNR** formed a monoclinic unit cell and the $P121/n1$ space group, whereas **TF-hNR** formed a monoclinic unit cell and the $C12/c1$ space group. The conjugated C–N bond lengths of **H-hNR** (1.358 and 1.359 Å) and **TF-hNR** (1.360 and 1.352 Å) indicated the delocalization of the positive charge. In addition, the slightly distorted and rigid structures of **H-hNR** and **TF-hNR** could probably render them highly fluorescent due to reducing aggregation between molecules.[14]

Photophysical Properties and DFT Calculations. The absorption and fluorescence data of **H-hNR** and **TF-hNR** in CH_2Cl_2, EtOH, and TE buffer are summarized in Table 1, and the corresponding spectra are shown in Figure 1 and Figures S5 and S6 of the Supporting Information. The maximum absorption wavelengths (λ_{abs}^{max}) of **H-hNR** in different solvents were in the visible light region, whereas the maximum fluorescence wavelengths (λ_{em}^{max}) were mainly in the deep-red region. Remarkably, **H-hNR** exhibited high QYs, particularly in CH_2Cl_2 and EtOH. Compared with previously reported dye **CP**[11a] (structure shown in Figure 2), **H-hNR**

Table 1. Photophysical Properties of H-hNR, TF-hNR, and CP[a]

dye	solvent	$\lambda_{abs}^{max}/\lambda_{em}^{max}$ (nm)	Stokes shift (cm^{-1})	ε ($M^{-1}cm^{-1}$)	Φ^a/Φ^b
H-hNR	CH_2Cl_2	619/642	579	133200	0.677/0.724
	EtOH	612/644	812	78200	0.576/0.618
	TE buffer	604/641	956	65500	0.310/0.282
TF-hNR	CH_2Cl_2	684/713	595	97100	0.310/0.336
	EtOH	680/725	913	54400	0.119/0.163
	TE buffer	672/716	914	47100	0.034/0.039
CP[11a]	CH_2Cl_2	618/648	749	80800	0.220/0.265
	TE buffer	598/658	1524	39000	0.010/0.009

[a]Conditions: Φ^a is the relative fluorescence quantum yield determined by using cresyl violet (ref 21) and zinc phthalocyanine (ref 22) as the standards; Φ^b is the absolute fluorescence quantum yield measured by using an integrating sphere.

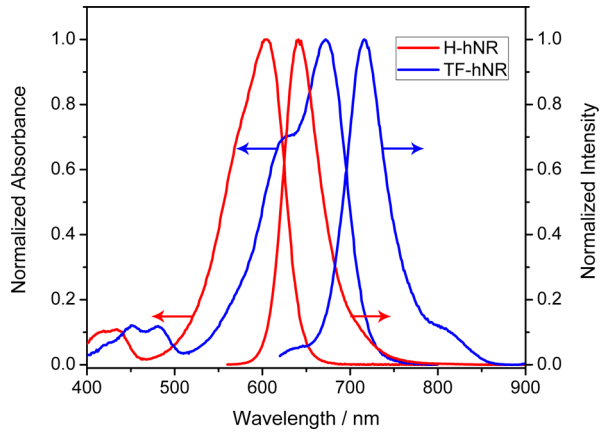

Figure 1. Normalized absorption and fluorescence spectra of **H-hNR** and **TF-hNR** in TE buffer.

DOI: 10.1021/acs.joc.6b00981
J. Org. Chem. 2016, 81, 7393–7399

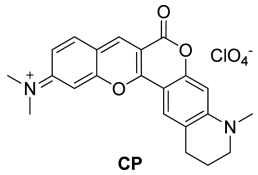

Figure 2. Molecular structure of **CP**.[11a]

exhibited a much higher quantum yield (Table 1). The replacement of the lactone group with an ethylene group might weaken the interaction with solvent, thus resulting in reduced nonradiative transitions.[12] Additionally, reduced ICT effect could also attribute to the high quantum yield of **H-hNR** due to the smaller Stokes shift of **H-hNR** in comparison with that of **CP**.[13] Previous studies have proved that the introduction of an electron-withdrawing group CF_3 at position 9 of xanthenes leads to dyes with longer absorption and emission because the electron-withdrawing group CF_3 could largely decrease the energy of excited state, resulting in a narrower bad gap and red-shifted absorption and emission.[7b,15] Compared with the absorption and fluorescence wavelengths of **H-hNR**, those of **TF-hNR** were extended to the deep-red and NIR regions, respectively. The QY of **TF-hNR** was high in CH_2Cl_2 but was sharply reduced from CH_2Cl_2 and EtOH to TE buffer because of its very narrow energy gap and enhanced nonradiative transitions in NIR fluorescent dyes.[17]

To further investigate the optical properties of **H-hNR**, **TF-hNR**, and **CP**, we performed DFT calculations at the B3LYP/6-31G level of theory by using the Gaussian 09 program package.[18] The calculated HOMOs and LUMOs of **H-hNR**, **TF-hNR**, and **CP** are shown in Figure 3, and the optimized

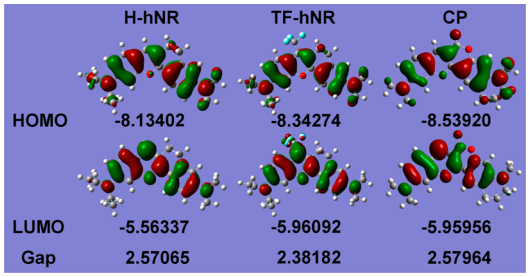

Figure 3. Spatial distributions of calculated HOMOs and LUMOs and HOMO/LUMO energy gaps (units, eV) of **H-hNR**, **TF-hNR** and **CP**.

structures are shown in Figure S7 of the Supporting Information. Compared with **CP**, **H-hNR** exhibited slightly higher HOMO and LUMO energy levels probably due to reduced ICT effect, while the energy gap was comparable to that of **CP**. In addition, the electron density of LUMOs was not localized in the ethylene part of **H-hNR**, while it was localized in the lactone part of **CP**, which further indicated the decreased ICT effect for **H-hNR**. As for **TF-hNR**, the HOMO and LUMO energy levels were decreased due to the electron-withdrawing group CF_3, thus resulting in narrower energy gap and red-shifted absorption and emission, which was in agreement with measured photophysical data (Table 1). The optimized structures (Figure S7 of the Supporting Information) further showed that **H-hNR** and **TF-hNR** exhibited twisted molecular structures while **CP** exhibited a planar structure, which probably had an important effect on the emissions of these dyes.

The effects of pH on the absorption spectra of **H-hNR** and **TF-hNR** were investigated in different Britton–Robinson (BR) buffers (40 mM, pH 2–11). The corresponding data are shown in Figure 4a and Figure S8 of the Supporting Information. The

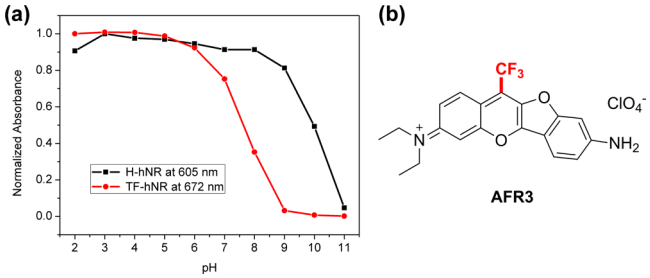

Figure 4. (a) pH-dependence of the normalized absorption of **H-hNR** and **TF-hNR**. (b) Molecular structure of **AFR3**.[15a]

absorption intensity of **H-hNR** varied slightly within the pH range of 2–8 but dropped sharply beginning from the pH value of 9. Such a decrease is attributed to the attachment of hydroxyl under highly alkaline environment conditions. For **TF-hNR**, the absorption intensity remained stable mainly under acidic conditions (pH 2–6) but dropped significantly when the pH value was higher than 7 as a result of the easier attachment of hydroxyl under alkaline environment conditions, which resulted from the high electron deficiency of the position directly connected to CF_3 of **TF-hNR**. The data on the effect of pH on **TF-hNR** is consistent with our previously reported data on **AFR3** (Figure 4b).[15a]

Considering that reduced glutathione (GSH) with high levels is present in live cells and GSH could react with reactive fluorophores, we tested the stability of **H-hNR** and **TF-hNR** in the presence of 10 mM GSH. After addition of 10 mM GSH for 10 min, the absorptions of **H-hNR** and **TF-hNR** were measured, and the corresponding data are summarized in Figure S9 of the Supporting Information. We could clearly see that the absorption intensity of **H-hNR** showed very little change after addition of 10 mM GSH. For **TF-hNR**, the absorption intensity slightly increased after addition of 10 mM GSH. These data further demonstrate that **H-hNR** and **TF-hNR** exhibit good stability in the presence of high levels of GSH.

Bioimaging and Cell Location. The cell uptake of **H-hNR** and **TF-hNR** was studied in A549 cells and HeLa cells by confocal laser scanning microscopy. We first performed cell-imaging experiments with different concentrations of **H-hNR** and **TF-hNR** (Figure 5). After incubation for 10 min, clear

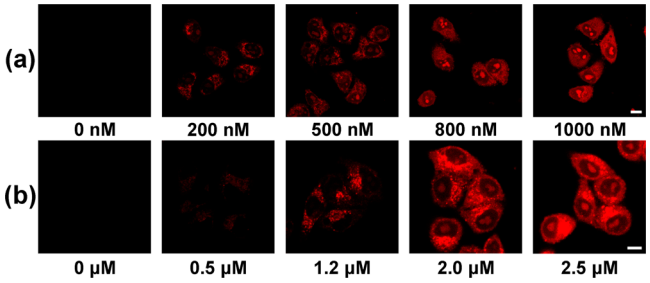

Figure 5. Confocal fluorescence microscopy images of HeLa cells stained with different concentrations of (a) **H-hNR** and (b) **TF-hNR**. Scale bar: 10 μm.

DOI: 10.1021/acs.joc.6b00981
J. Org. Chem. 2016, 81, 7393–7399

fluorescence of **H-hNR** in the nucleolus and cytoplasm can be detected at a concentration as low as 200 nM. For **TF-hNR**, an optimized concentration at 2 μM was adopted to obtain clear fluorescence in the nucleolus and cytoplasm. In addition, cell imaging experiments at different time points were also conducted, and the corresponding imaging of **H-hNR** and **TF-hNR** was obtained (Figure 6 and Figure S10 of the

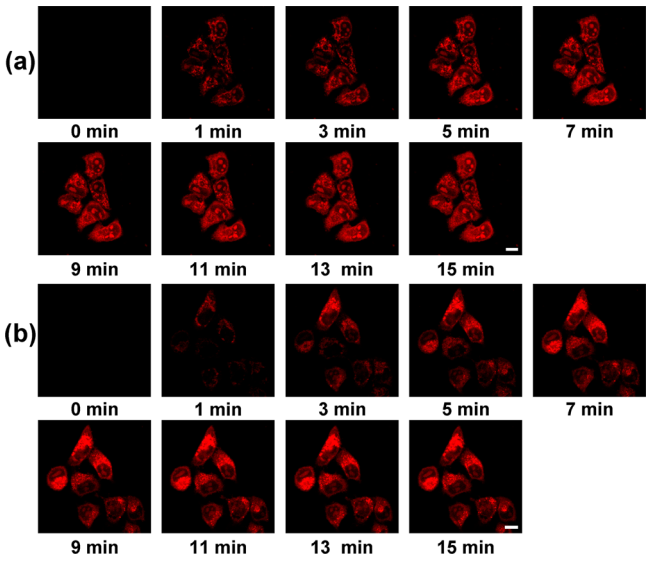

Figure 6. Confocal fluorescence microscopy images of HeLa cells stained with (a) **H-hNR** (0.8 μM) and (b) **TF-hNR** (2 μM) at different time points. Scale bar: 10 μm.

Supporting Information). For most of the fluorophore-staining nucleoli, a long incubation time (tens of minutes or even several hours) is needed to obtain satisfactory images of nucleolus imaging in live cells.[19] Parker et al.[19b] synthesized a europium complex staining nucleolus in live cells in 1 h. Tang's group reported a α-cyanostilbene derivative (ASCP) with a dual-color nucleolus and mitochondria imaging at up to 30 min incubation.[19h] Compared with these fluorophores, **H-hNR** and **TF-hNR** could easily enter live cells with rapid localization. The fluorescence intensities in the nucleolus and cytoplasm almost reached saturation in approximately 9 min for both **H-hNR** and **TF-hNR**, indicating that they had excellent cell plasma and nuclear membrane permeability.

DNase and RNase digest experiments were performed in fixed A549 cells to confirm the localization of fluorescence in the nucleolus. As shown in Figure 7, in the presence of DNase, the fluorescence intensities of **H-hNR** and **TF-hNR** in the nucleoli and cytoplasm remained almost the same, whereas the fluorescence intensity in the nucleolus slightly decreased. By contrast, upon treatment with RNase, the fluorescence intensity in nucleoli significantly dropped, whereas the fluorescence intensity in the cytoplasm was slightly enhanced; SYTO RNASelect showed almost the same tendency in the digest experiments. The fluorescence in the nucleolus almost vanished for DAPI in the presence of DNase, whereas the fluorescence basically remained the same upon treatment with RNase. These imaging data demonstrated that **H-hNR** and **TF-hNR** stain nucleolus via the noncovalent interaction with nucleolar RNA.

For the fluorescence obtained in cytoplasm, two commercial dyes, MitoTracker Green FM (MTG) and LysoTracker Green DND-26 (LTG), were used for costaining with **H-hNR** or **TF-hNR** to confirm the localization. Colocalization imaging data (Figure 8, Figure S11, and Table S3 of the Supporting

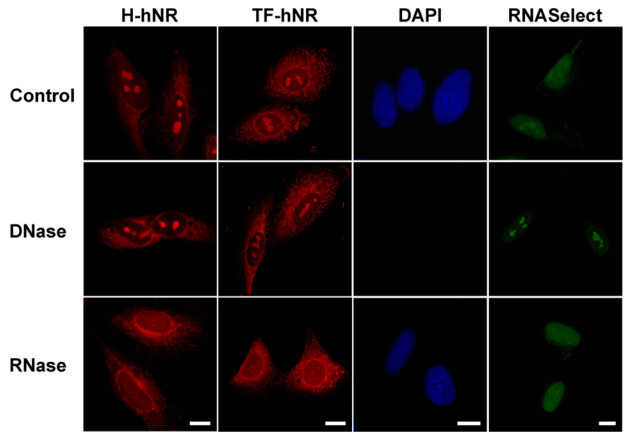

Figure 7. DNase and RNase digest experiments. Scale bar: 10 μm.

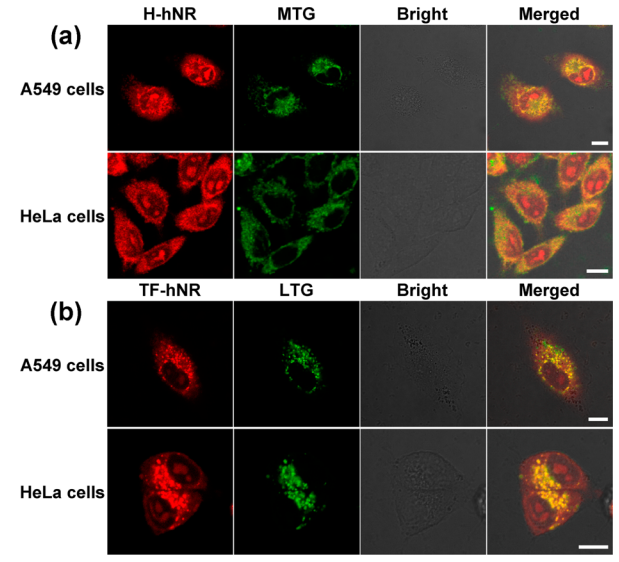

Figure 8. Confocal fluorescence microscopy images of A549 and HeLa cells (a) stained with MTG (100 nM) and **H-hNR** (0.8 μM) and (b) stained with LTG (200 nM) and **TF-hNR** (2 μM). Scale bar: 10 μm.

Information) showed that **H-hNR** mainly located in the mitochondria with good overlap with MTG, while the fluorescence observed for **TF-hNR** in cytoplasm was mainly associated with lysosomes. Notably, the fluorescence of **TF-hNR** in lysosomes was brighter than that in the nucleolus because **TF-hNR** showed strong emission under acidic conditions (Figure 4a) and lysosomes are acidic organelles (pH 4.6–5.0).[20]

Photostability and Cytotoxicity. The photostability and cytotoxicity of **H-hNR** and **TF-hNR** are crucial indicators of synthesized dyes for imaging-related biological applications. The photostability of **H-hNR** and **TF-hNR** was evaluated in HeLa cells fixed in prechilled methanol by continuous irradiation with laser. Figure 9 showed that the intensity of **H-hNR** and **TF-hNR** decreased to 90% after 30 min of continuous irradiation. As a comparison, however, over 90% of the initial fluorescence intensity of commercial SYTO RNASelect was significantly decreased only in 10 min, and the intensity of MTG and LTG decreased to 6.4% and 51.2%

DOI: 10.1021/acs.joc.6b00981
J. Org. Chem. 2016, 81, 7393–7399

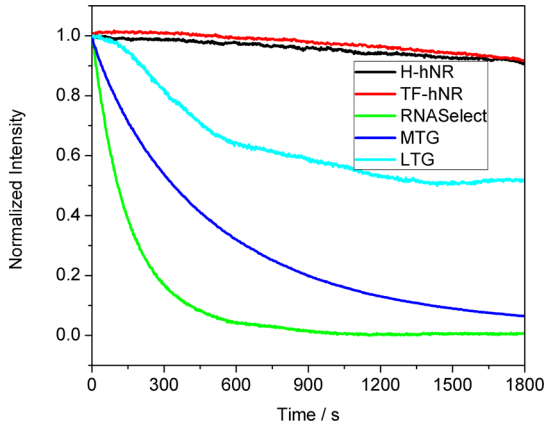

Figure 9. Photostability of **H-hNR**, **TF-hNR**, SYTO RNASelect, MTG, and LTG in HeLa cells fixed with prechilled methanol. Irradiation conditions: for H-hNR, 640 nm laser, laser power 8%; for TF-hNR, 640 nm laser, laser power 40%; for SYTO RNASelect, 488 nm laser, laser power 8%; for MTG, 488 nm laser, laser power 8%; for LTG, 488 nm laser, laser power 8%.

after 30 min of continuous irradiation, respectively. As for evaluating the cytotoxicity of **H-hNR** and **TF-hNR**, standard MTT (3-(4,5-dimethylthiazol-2-yl)-2,5-diphenyl-2*H*-tetrazolium) assays were performed in A549 and HeLa cells. After incubation in HeLa cells for 24 h, the data showed that **H-hNR** and **TF-hNR** exhibited negligible cytotoxicity at low concentrations (Figure S12 of the Supporting Information).

CONCLUSIONS

In summary, we successfully synthesized two xanthene dyes (i.e., **H-hNR** and **TF-hNR**) with deep-red and NIR emissions by facile and straightforward methods. The X-ray diffraction structures, DFT calculations, and photophysical properties of **H-hNR** demonstrated that the ethylene group in the skeleton can efficiently improve the QYs in polar solution. Cell-imaging studies reveal that **H-hNR** and **TF-hNR** located in nucleolus and mitochondria (or lysosomes) in both A549 and HeLa cells with short incubation time and low concentration. Moreover, these two dyes show excellent photostability and low cytotoxicity. This work may provide an opportunity for the construction of other xanthene dyes with high QYs for live cell imaging.

EXPERIMENTAL SECTION

General Methods. All commercial chemicals were used as received without further purification. SYTO RNASelect, DAPI, MitoTracker Green FM (MTG), and LysoTracker Green DND-26 (LTG) were purchased from Invitrogen (USA). DNase and DNase-free RNase were purchased from Takara. ^{1}H NMR (400 MHz), ^{13}C NMR (100 MHz), and ^{19}F NMR (376 MHz) spectra were recorded on a 400, 100, and 376 MHz instrument, respectively, with tetramethylsilane as an internal standard. Electrospray ionization high-resolution mass spectra (ESI-HRMS) were measured by Fourier transform ion cyclotron resonance mass spectrometry (FTICR-MS). All absorption and fluorescence spectra in this work were obtained at room temperature, respectively.

Relative Fluorescence Quantum Yield Measurement. Cresyl violet in methanol (Φ = 0.54)[21] and zinc phthalocyanine in toluene (containing 1% pyridine; Φ = 0.30)[22] were chosen as the standards for **H-hNR** and **TF-hNR**, respectively. The fluorescence quantum yields of **H-hNR** and **TF-hNR** were calculated according to the following equation: $\Phi_x = \Phi_{st}[n_x^2/n_{st}^2][G_x/G_{st}]$, where Φ is the fluorescence quantum yield, G is the gradient from the plot of integrated fluorescence intensity versus absorbance, n is the refractive index of different solvents. The subscript "st" and "x" refer to the standard and unknown and dye, respectively. The excitation wavelengths (λ_{ex}) for QY measurement of **H-hNR** and **TF-hNR** were 540 and 605 nm, respectively, and the absorbance values of all dyes were below 0.08. The related data are shown in Figure S4 of the Supporting Information.

Imaging. Two tumor cell lines, A549 (human lung adenocarcinoma epithelial cell line) and HeLa (human cervical adenocarcinoma epithelial cell line) were used to perform the imaging-related experiments. A549 and HeLa cells were cultured in McCoy's 5A and Dulbecco's modified Eagle medium (DMEM), respectively, containing 10% fetal bovine serum (FBS) including 1% antibiotics (50 unit/mL penicillin, and 50 mg/mL of streptomycin) under 5% CO_2 at 37 °C in a humidified incubator. After incubation for 24 h, fresh culture media (containing 0.8 μM **H-hNR** and 2 μM **TF-hNR**) were added into the confocal dishes, and the confocal dishes were incubated for 10 min prior to conduct the experiments. As for colocalization experiments, apart from the above-mentioned concentrations of **H-hNR** and **TF-hNR** in the fresh culture media, commercially available mitochondria-specific green fluorescent dye MitoTracker Green FM (MTG, 100 nM) and lysosome-specific green fluorescent dye LysoTracker Green DND-26 (LTG, 200 nM) were also contained to perform the corresponding imaging experiments. All of the confocal dishes were washed with PBS (phosphate-buffered saline) before imaging. Fluorescent images were acquired with a confocal laser scanning microscopy (for DAPI, excited at 405 nm, DAPI channel; for SYTO RNASelect, MTG, and LTG, excited at 488 nm, FITC channel; for **H-hNR** and **TF-hNR**, excited at 640 nm, Cy5 channel.). Images were processed by NIS-Elements Viewer 3.20. For photostability, SYTO RNASelect, MTG, and LTG were continuous irradiated with a 488 nm laser, and a 640 nm laser was used for **H-hNR** and **TF-hNR**.

DNase and RNase Digest Experiments. A549 cells were fixed in prechilled methanol at −20 °C for 1 min, and then the cells were washed with l mL of PBS with 1% Triton X-100 for 1 min at room temperature to permeabilize the cell membrane. After the solution was washed twice with PBS, 1 mL of PBS (containing 0.8 μM **H-hNR**, 2 μM **TF-hNR**, 1 μg/mL of DAPI, and 0.5 μM SYTO RNASelect) solution was added. Then incubation for 20 min at room temperature, they were rised clean by PBS twice. A total of 1 mL of PBS (as the control experiment), 1 mL of DNase solution (20 u/mL in PBS), and 1 mL of DNase-free RNase solution (25 μg/mL in PBS) were added into the three other dishes. After incubation for 2 h under 5% CO_2 at 37 °C in a humidified incubator, the cells were rinsed clean by PBS twice more before imaging. To obtain the fluorescent imaging pictures under the same conditions, equal exposure time and laser intensity were used for the control, DNase, and RNase experiments.

Synthesis of H-hNR. Compound **H-hNR** was synthesized following our previous method.[15a] Concentrated H_2SO_4 (5 mL) was initially poured into a round-bottomed flask, and the solution was stirred at room temperature. Then compounds **2** (189 mg, 1.0 mmol) and **6** (193 mg, 1.0 mmol) were successively added, and the mixture was heated at 100 °C for 4 h. After being cooled to room temperature, the mixture was poured into ice−water. Perchloric acid (1 mL) was slowly added into the solution, and the resulting precipitate was filtered and washed with generous amounts of water. The sample was dried and purified by silica gel chromatography using $v(CH_2Cl_2)$/$v(CH_3OH)$ = 30:1 as the eluent to obtain green solid **H-hNR** (360 mg, 81%). ^{1}H NMR (400 MHz, DMSO-d_6): δ (ppm) 8.35 (s, 1H), 8.09 (d, J = 9.1 Hz, 1H), 7.77 (d, J = 9.2 Hz, 1H), 7.22 (dd, J = 9.2, 2.1 Hz, 1H), 7.16 (s, 1H), 6.90 (d, J = 9.2 Hz, 1H), 6.77 (s, 1H), 3.61 (q, J = 7.0 Hz, 4H), 3.19 (s, 6H), 2.98 (s, 4H), 1.22 (t, J = 7.0 Hz, 6H). ^{13}C NMR (100 MHz, DMSO-d_6): δ (ppm) 164.5, 156.6, 155.0, 153.4, 145.6, 144.6, 130.7, 128.9, 120.2, 115.1, 114.9, 112.8, 111.9, 110.8, 95.8, 44.8, 39.9 (overlapped with DMSO-d_6), 27.1, 25.1, 12.4. HRMS (ESI): calcd for $[C_{23}H_{27}N_2O]^+$ m/z 347.21179 $[M]^+$, found m/z 347.21180.

Synthesis of TF-hNR. The compound **TF-hNR** was synthesized following our previous method.[15a] Concentrated H_2SO_4 (10 mL) was initially poured into a round-bottomed flask, and the solution was

DOI: 10.1021/acs.joc.6b00981
J. Org. Chem. 2016, 81, 7393−7399

stirred at room temperature. Then compounds **2** (378 mg, 2.0 mmol) and **5** (522 mg, 2.0 mmol) were successively added, and the mixture was heated at 100 °C for 12 h. After being cooled to room temperature, the mixture was poured into ice−water. Perchloric acid (2 mL) was slowly added into the solution, and the resulting precipitate was filtered and washed with generous amounts of water. The sample was dried and purified by silica gel chromatography using $v(CH_2Cl_2)/v(CH_3OH)$ = 70:1 as the eluent to obtain green solid **TF-hNR** (164 mg, 16%). ^{1}H NMR (400 MHz, DMSO-d_6): δ (ppm) 8.20 (d, J = 9.3 Hz, 1H), 7.81 (dd, J = 9.4, 2.1 Hz, 1H), 7.24 (dt, J = 9.5, 2.6 Hz, 2H), 7.00 (dd, J = 9.3, 2.5 Hz, 1H), 6.84 (d, J = 2.3 Hz, 1H), 3.61 (q, J = 7.0 Hz, 4H), 3.28 (s, 6H), 3.11 (t, J = 6.5 Hz, 2H), 2.99 (t, J = 7.1 Hz, 2H), 1.22 (t, J = 7.0 Hz, 6H). ^{13}C NMR (100 MHz, DMSO-d_6): δ (ppm) 164.9, 156.1, 155.9, 152.4, 146.7, 135.7 (q, J = 303 Hz), 130.6, 126.5 (q, J = 5 Hz), 124.5, 121.7, 120.5 (q, J = 3 Hz), 115.4, 113.4 (q, J = 5 Hz), 110.6, 109.2, 96.7, 44.8, 40.3, 26.5, 23.6 (q, J = 4 Hz), 12.5. ^{19}F NMR (376 MHz, DMSO-d_6): δ (ppm) − 54.0 (s, 3F). HRMS (ESI): calcd for $[C_{24}H_{26}F_3N_2O]^+$ m/z 415.19917 $[M]^+$, found m/z 415.19917.

■ ASSOCIATED CONTENT

Supporting Information

The Supporting Information is available free of charge on the ACS Publications website at DOI: 10.1021/acs.joc.6b00981.

X-ray data for **H-hNR** (CIF)
X-ray data for **TF-hNR** (CIF)
Photophysical data; cell data; details of DFT calculations (absolute energy and atomic coordinates); NMR spectra of new compounds; HR-MS spectra(PDF)

■ AUTHOR INFORMATION

Corresponding Author

*E-mail: wmliu@mail.ipc.ac.cn.

Present Address

§(B.Z.) Key Laboratory of Bioorganic Phosphorus Chemistry & Chemical Biology (Ministry of Education), Department of Chemistry, Tsinghua University, Beijing, 100084, China.

Notes

The authors declare no competing financial interest.

■ ACKNOWLEDGMENTS

This work was supported by the National Natural Science Foundation of China (Grant Nos. 21373250 and 61227008) and 973 Program (No. 2014CB932600). All calculations were performed on the cluster of Key Laboratory of Theoretical and Computational Photochemistry, Ministry of Education, China.

■ REFERENCES

(1) Brewer, T. F.; Chang, C. J. *J. Am. Chem. Soc.* **2015**, *137*, 10886.
(2) Shieh, P.; Siegrist, M. S.; Cullen, A. J.; Bertozzi, C. R. *Proc. Natl. Acad. Sci. U. S. A.* **2014**, *111*, 5456.
(3) Zhang, H.; Fan, J.; Wang, J.; Dou, B.; Zhou, F.; Cao, J.; Qu, J.; Cao, Z.; Zhao, W.; Peng, X. *J. Am. Chem. Soc.* **2013**, *135*, 17469.
(4) (a) Cheng, Y.; Li, G.; Liu, Y.; Shi, Y.; Gao, G.; Wu, D.; Lan, J.; You, J. *J. Am. Chem. Soc.* **2016**, *138*, 4730. (b) Kaloyanova, S.; Zagranyarski, Y.; Ritz, S.; Hanulová, M.; Koynov, K.; Vonderheit, A.; Müllen, K.; Peneva, K. *J. Am. Chem. Soc.* **2016**, *138*, 2881.
(5) (a) Weissleder, R. *Nat. Biotechnol.* **2001**, *19*, 316. (b) Yuan, L.; Lin, W.; Zheng, K.; He, L.; Huang, W. *Chem. Soc. Rev.* **2013**, *42*, 622. (c) Guo, Z.; Park, S.; Yoon, J.; Shin, I. *Chem. Soc. Rev.* **2014**, *43*, 16.
(6) (a) Chen, X.; Pradhan, T.; Wang, F.; Kim, J. S.; Yoon, J. *Chem. Rev.* **2012**, *112*, 1910. (b) Zheng, H.; Zhan, X.-Q.; Bian, Q.-N.; Zhang, X.-J. *Chem. Commun.* **2013**, *49*, 429.
(7) (a) Shi, J. M.; Zhang, X. P.; Neckers, D. C. *Tetrahedron Lett.* **1993**, *34*, 6013. (b) Sauer, M.; Han, K. T.; Mueller, R.; Schulz, A.; Tadday, R.; Seeger, S.; Wolfrum, J.; Arden-Jacob, J.; Deltau, G.; Marx, N. J.; Drexhage, K. H. *J. Fluoresc.* **1993**, *3*, 131. (c) Kolmakov, K.; Wurm, C. A.; Hennig, R.; Rapp, E.; Jakobs, S.; Belov, V. N.; Hell, S. W. *Chem. - Eur. J.* **2012**, *18*, 12986.
(8) (a) Yuan, L.; Lin, W.; Yang, Y.; Chen, H. *J. Am. Chem. Soc.* **2012**, *134*, 1200. (b) Yuan, L.; Lin, W.; Zhao, S.; Gao, W.; Chen, B.; He, L.; Zhu, S. *J. Am. Chem. Soc.* **2012**, *134*, 13510. (c) Xiong, X.; Song, F.; Chen, G.; Sun, W.; Wang, J.; Gao, P.; Zhang, Y.; Qiao, B.; Li, W.; Sun, S.; Fan, J.; Peng, X. *Chem. - Eur. J.* **2013**, *19*, 6538. (d) Liu, W.; Fan, C.; Sun, R.; Xu, Y.-J.; Ge, J.-F. *Org. Biomol. Chem.* **2015**, *13*, 4532. (e) Chen, H.; Dong, B.; Tang, Y.; Lin, W. *Chem. - Eur. J.* **2015**, *21*, 11696. (f) Chen, H.; Lin, W.; Jiang, W.; Dong, B.; Cui, H.; Tang, Y. *Chem. Commun.* **2015**, *51*, 6968.
(9) (a) Fu, M.; Xiao, Y.; Qian, X.; Zhao, D.; Xu, Y. *Chem. Commun.* **2008**, 1780. (b) Koide, Y.; Urano, Y.; Hanaoka, K.; Terai, T.; Nagano, T. *ACS Chem. Biol.* **2011**, *6*, 600. (c) Kushida, Y.; Nagano, T.; Hanaoka, k. *Analyst* **2015**, *140*, 685. (d) Chai, X.; Cui, X.; Wang, B.; Yang, F.; Cai, Y.; Wu, Q.; Wang, T. *Chem. - Eur. J.* **2015**, *21*, 16754. (e) Fukazawa, A.; Suda, S.; Taki, M.; Yamaguchi, E.; Grzybowski, M.; Sato, Y.; Higashiyama, T.; Yamaguchi, S. *Chem. Commun.* **2016**, *52*, 1120.
(10) (a) Jiao, C.; Huang, K.-W.; Wu, J. *Org. Lett.* **2011**, *13*, 632. (b) Bochkov, A. Y.; Akchurin, I. O.; Dyachenko, O. A.; Traven, V. F. *Chem. Commun.* **2013**, *49*, 11653. (c) Chevalier, A.; Renard, P.-Y.; Romieu, A. *Chem. - Eur. J.* **2014**, *20*, 8330. (d) Katori, A.; Azuma, E.; Ishimura, H.; Kuramochi, K.; Tsubaki, K. *J. Org. Chem.* **2015**, *80*, 4603.
(11) (a) Zhou, B.; Liu, W.; Zhang, H.; Wu, J.; Liu, S.; Xu, H.; Wang, P. *Biosens. Bioelectron.* **2015**, *68*, 189. (b) Liu, W.; Zhou, B.; Niu, G.; Ge, J.; Wu, J.; Zhang, H.; Xu, H.; Wang, P. *ACS Appl. Mater. Interfaces* **2015**, *7*, 7421.
(12) Lakowicz, J. R. *Principles of Fluorescence Spectroscopy*, 2nd ed.; Kluwer Academic: New York, 1999.
(13) (a) Myung Kim, H.; Rae Cho, B. *Chem. Commun.* **2009**, 153. (b) Shao, J.; Guan, Z.; Yan, Y.; Jiao, C.; Xu, Q.-H.; Chi, C. *J. Org. Chem.* **2011**, *76*, 780. (c) Felouat, A.; D'Aléo, A.; Charaf-Eddin, A.; Jacquemin, D.; Le Guennic, B.; Kim, E.; Lee, K. J.; Woo, J. H.; Ribierre, J.-C.; Wu, J. W.; Fages, F. *J. Phys. Chem. A* **2015**, *119*, 6283.
(14) (a) Birks, J. B. *Photophysics of Aromatic Molecules*; John Wiley & Sons, Ltd.:London, 1970. (b) Tang, B. Z.; Qin, A. *Aggregation-Induced Emission: Fundamentals*; John Wiley & Sons Ltd.: West Sussex, 2013.
(15) (a) Niu, G.; Liu, W.; Wu, J.; Zhou, B.; Chen, J.; Zhang, H.; Ge, J.; Wang, Y.; Xu, H.; Wang, P. *J. Org. Chem.* **2015**, *80*, 3170. (b) Anzalone, A. V.; Wang, T. Y.; Chen, Z. X.; Cornish, V. W. *Angew. Chem., Int. Ed.* **2013**, *52*, 650. (c) Sauer, M.; Han, K. T.; Müller, R.; Nord, S.; Schulz, A.; Seeger, S.; Wolfrum, J.; Arden-Jacob, J.; Deltau, G.; Marx, N. J.; Zander, C.; Drexhage, K. H. *J. Fluoresc.* **1995**, *5*, 247.
(16) Niu, G.; Liu, W.; Xiao, H.; Zhang, H.; Chen, J.; Dai, Q.; Ge, J.; Wu, J.; Wang, P. *Chem. - Asian J.* **2016**, *11*, 498.
(17) (a) Sommer, J. R.; Shelton, A. H.; Parthasarathy, A.; Ghiviriga, I.; Reynolds, J. R.; Schanze, K. S. *Chem. Mater.* **2011**, *23*, 5296. (b) Chen, J.; Liu, W.; Zhou, B.; Niu, G.; Zhang, H.; Wu, J.; Wang, Y.; Ju, W.; Wang, P. *J. Org. Chem.* **2013**, *78*, 6121.
(18) Frisch, M. J.; Trucks, G. W.; Schlegel, H. B.; Scuseria, G. E.; Robb, M. A.; Cheeseman, J. R.; Montgomery, J. A., Jr.; Vreven, T.; Kudin, K.; Burant, J. C. et al. *Gaussian 09*, revision A.02; Gaussian, Inc.: Wallingford, CT, 2009..
(19) (a) Li, Q.; Kim, Y.; Namm, J.; Kulkarni, A.; Rosania, G. R.; Ahn, Y.-H.; Chang, Y.-T. *Chem. Biol.* **2006**, *13*, 615. (b) Yu, J.; Parker, D.; Pal, R.; Poole, R. A.; Cann, M. J. *J. Am. Chem. Soc.* **2006**, *128*, 2294. (c) Stevens, N.; O'Connor, N.; Vishwasrao, H.; Samaroo, D.; Kandel, E. R.; Akins, D. L.; Drain, C. M.; Turro, N. J. *J. Am. Chem. Soc.* **2008**, *130*, 7182. (d) Li, Z.; Sun, S.; Yang, Z.; Zhang, S.; Zhang, H.; Hu, M.; Cao, J.; Wang, J.; Liu, F.; Song, F.; Fan, J.; Peng, X. *Biomaterials* **2013**, *34*, 6473. (e) Song, G.; Sun, Y.; Liu, Y.; Wang, X.; Chen, M.; Miao, F.; Zhang, W.; Yu, X.; Jin, J. *Biomaterials* **2014**, *35*, 2103. (f) Zhang, S.; Fan, J.; Li, Z.; Hao, N.; Cao, J.; Wu, T.; Wang, J.; Peng, X. *J. Mater. Chem. B* **2014**, *2*, 2688. (g) Guo, L.; Chan, M. S.; Xu, D.; Tam, D. Y.; Bolze, F.; Lo, P. K.; Wong, M. S. *ACS Chem. Biol.* **2015**, *10*, 1171.

DOI: 10.1021/acs.joc.6b00981
J. Org. Chem. 2016, 81, 7393−7399

(h) Yu, C. Y. Y.; Zhang, W.; Kwok, R. T. K.; Leung, W. T.; Lam, J. W. Y.; Tang, B. Z. *J. Mater. Chem. B* **2016**, *4*, 2614.
(20) Luzio, J. P.; Pryor, P. R.; Bright, N. A. *Nat. Rev. Mol. Cell Biol.* **2007**, *8*, 622.
(21) Magde, D.; Brannon, J. H.; Cremers, T. L.; Olmsted, J. *J. Phys. Chem.* **1979**, *83*, 696.
(22) Vincett, P. S.; Voigt, E. M.; Rieckhoff, K. E. *J. Chem. Phys.* **1971**, *55*, 4131.

DOI: 10.1021/acs.joc.6b00981
J. Org. Chem. 2016, 81, 7393−7399